SECED 2023 Conference
Earthquake Engineering & Dynamics for a Sustainable Future
14-15 September 2023, Cambridge, UK

DYNAMIC CHARACTERISTICS OF JACKET-SUPPORTED OFFSHORE WIND TURBINES

Zeyad KHALIL[1], Peter J. STAFFORD[2] & Ahmed Y. ELGHAZOULI[3]

Abstract: *Wind energy is continuously growing to be a major source of clean renewable energy. Many countries worldwide have set ambitious targets to reach net-zero carbon emissions, with offshore wind energy production regarded as a key contributor. Such vital structures have been recently constructed in seismically active regions globally, along with planned future expansion in areas of moderate-to-high seismic activity. However, there has been relatively limited information on the long-term performance of large-scale offshore wind turbines under earthquake loading. There is therefore a need to understand the performance of this type of structure under such events. This study focuses on the assessment of the dynamic characteristics of relevance to the seismic performance of large-scale jacket-supported turbines with a rated power of at least 10 MW. Although this range represents the future trend in offshore wind developments, it has received little attention compared to monopile-supported offshore turbines. The performance of a four-legged, x-braced reference jacket structure supporting a 10 MW turbine constructed in a layered sand soil profile is investigated to provide initial insights that would aid the detailed evaluation of the seismic response of such structural systems.*

Introduction

Wind energy is continuously growing to be a major source of clean renewable energy nowadays where countries worldwide have set ambitious targets to reach net-zero carbon emissions, with offshore wind energy production regarded as a key contributor. The recent geopolitical traction and the challenges associated with climate change have highlighted the strategic importance of achieving diversification of energy sources through the deployment of renewables to allow for safeguarding the security of energy supply, elimination and reduction of adverse weather patterns, and avoidance of single energy source dependency (GWEC, 2022). Offshore wind energy production can play a major part to achieve such objectives. According to recently available information, offshore wind capacity has been increasing in the last two decades adding around 21 GW in 2021. This marks it as a record year for the offshore wind industry, contributing to nearly a quarter of the total installed wind energy capacity and nearly three times the amount installed in 2020, bringing the total global offshore wind capacity to 57.2 GW as shown in Figure 1 (WFA, 2022; GWEC, 2022).

Inevitably, with such worldwide momentum for adopting offshore wind energy sources, offshore wind farms have been very recently constructed in seismically active regions globally, along with ambitious future expansion plans in countries of moderate-to-high seismic activity (e.g., Italy, Greece, Taiwan, Japan, China, United States, and others) (GWEC, 2022; Bhattacharya *et al.*, 2021). There is, however, generally limited information on the long-term performance of large-scale offshore wind turbines under earthquake loading. This raises the need to understand the dynamic characteristics and response of such structures under such severe seismic events, in addition to other types of loads including operational mechanical loads, wind, and wave loading. Such understanding would help ensure the resilience of these assets as communities become increasingly dependent on them, in addition to evaluating and managing the risks associated with their exposure to such extreme environmental hazard scenarios.

This paper focuses on the assessment of the dynamic characteristics of relevance to the seismic performance of large-scale jacket-supported turbines of rated power of and exceeding 10 MW. This range represents the future trend of offshore wind developments and have received little attention in the literature compared to monopile-supported offshore turbines. The performance of a four-legged, x-braced reference jacket structure supporting a 10 MW turbine constructed in a

[1] PhD Student, Imperial College London, London, UK, zeyad.khalil19@imperial.ac.uk
[2] Professor of Engineering Seismology, Imperial College London, London, UK
[3] Professor of Structural Engineering, Imperial College London, London, UK

layered sand soil profile is investigated in order to provide initial insights that would aid the proper evaluation of the seismic structural response of such structures.

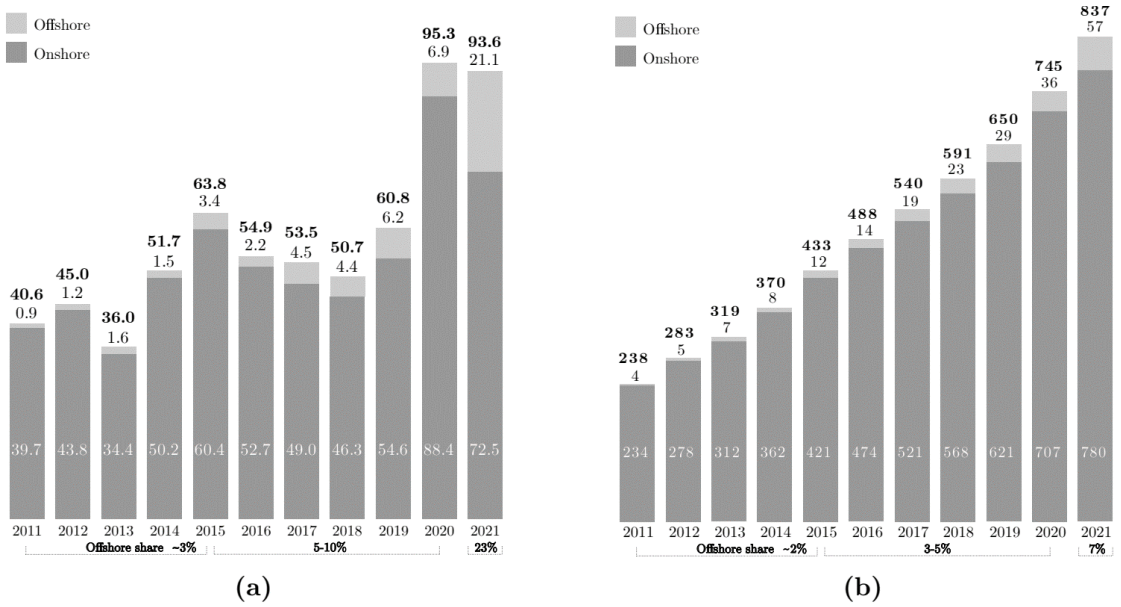

Figure 1: Global wind power capacity of new yearly installations (2011-2021): 21): (a) New yearly installations, and (b) Total cumulative installations. Data source: (GWEC, 2022).

Model Description

The INNWIND.EU jacket-supported 10 MW reference wind turbine model (RWT) is investigated (Von Borstel, 2013; Jensen *et al.*, 2017) herein as a representative example of large-scale jacket-supported OWTs. The wind turbine tower is based on a modified version of the DTU 10 MW RWT (Bak *et al.*, 2013), where the main tower properties are shown in Table 1. The tower is composed of 9 different conical sections where the outer diameter is varying between 7.67 m at the bottom of the tower to 5.5 m at the top. The wall thickness ranges between 38 mm at the base and 26 mm at the top, with the diameter-to-thickness ratio varying between 222 and 236.

Description	**Value**	**Unit**
Rated Power	10	MW
Cut-in, cut-out and rated wind speeds	4, 25 and 11.4	m/s
Minimum and maximum rotor speed	6 and 9.6	rpm
Rotor Diameter	178.33	m
Tower Height	89.63	m
RNA mass	676,723	kg
RNA Moment of Inertia about the x-axis	1.66×10^8	$kg.m^2$
RNA Moment of Inertia about the y- and z-axes	1.27×10^8	$kg.m^2$
Tower mass	1.27×10^8	$kg.m^2$
Overall mass (Tower + RNA)	1,105,924	kg
Young's modulus of steel	210	GPa

Table 1: Modified DTU RWT tower properties (Von Borstel, 2013).

The reference jacket supporting the 10 MW RWT is a four-legged structure with four levels of X-braces and one level of horizontal bracing provided at the bottom of the jacket supported on piles. The main properties of the jacket are shown in Table 2. The width of the jacket varies from 34 m at the base to around 14 m at the top with a height of 68 m. The jacket consists of 28 different cross-sections with diameters ranging from 832 to 1400 mm and thicknesses varying between 16 and 120 mm. The jacket is supported on piles penetrating to a depth of 40 m below the seabed, where each pile has a diameter of 2.4 m and a thickness ranging from 32 to 52 mm.

Description	Value	Unit
Base Width	34	m
Top Width	14	m
Jacket legs outer diameter	1400	mm
Jacket legs wall thickness	42-120	mm
Number of X-braces level	4	-
X-braces outer diameters	832-1088	mm
X-braces wall thickness	16-44	mm
Horizontal braces outer diameter	1040-1044	mm
Horizontal braces wall thickness	20-22	mm
Jacket structure mass	1,186,550	kg
Young's modulus of steel	210	GPa

Table 2: INNWIND.EU reference jacket properties (Jensen et al., 2017; Von Borstel, 2013).

The reference wind turbine is modelled with finite elements in the commercial software package ABAQUS (Dassault Systèmes, 2022) using beam elements, where the geometry of the model can be shown in Figure 2. The RNA has been modelled as a lumped mass incorporating rotational moments of inertia at the tower top without explicit modelling of the hub and rotor blades. A layered sandy soil profile is assumed of varying submerged unit weight ranging from 9 to 11 kN/m^3 and an angle of internal friction of 35°. The interaction between the piles and the surrounding soil is initially modelled using the traditional beam on nonlinear Winkler foundation (BNWF) method where the soil resistance, both in vertical and horizontal directions, is represented using a set of translational springs. The soil curves representing the load-displacement relationship for the soil-pile end bearing resistance (q-z), shaft resistance (t-z) and lateral resistance (p-y) are derived according to API RP 2A-WSD (API, 2007).

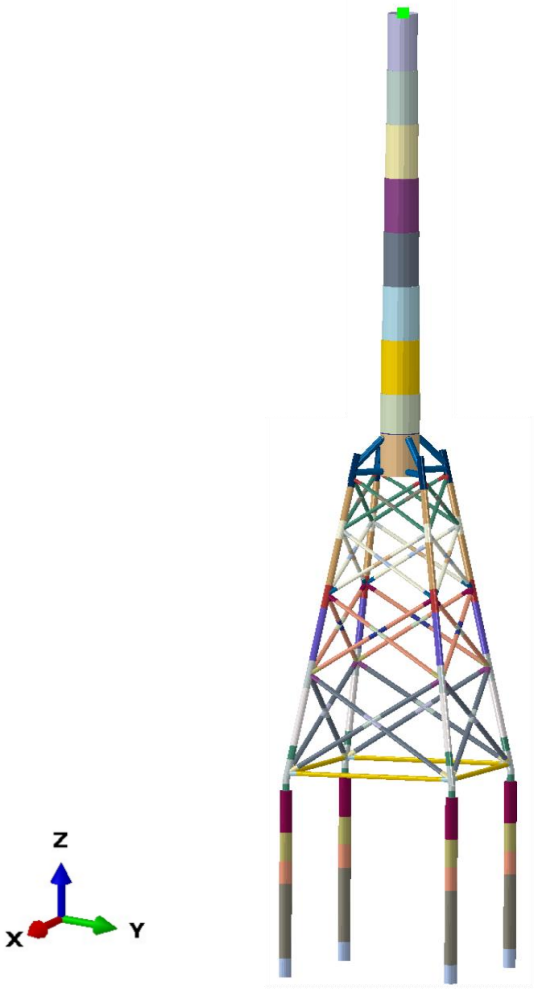

Figure 2: INNWIND.EU 10 MW reference wind turbine model.

Modal Analysis

Modal analysis for the previously described model including the tower, jacket, piles and soil springs has been first conducted using the nominal values for the material properties and cross-section dimensions to examine the natural vibration periods of the system and estimate the dynamic characteristics of the structure. The first and second bending modes of vibration in the two horizontal directions, in addition to the first torsional and vertical modes, are shown in Figure 3, and their corresponding natural frequencies, periods and mass participation ratios are reported in Table 3, which are in a relatively good match with other reported values with some expected deviations in higher modes due to modelling assumptions.

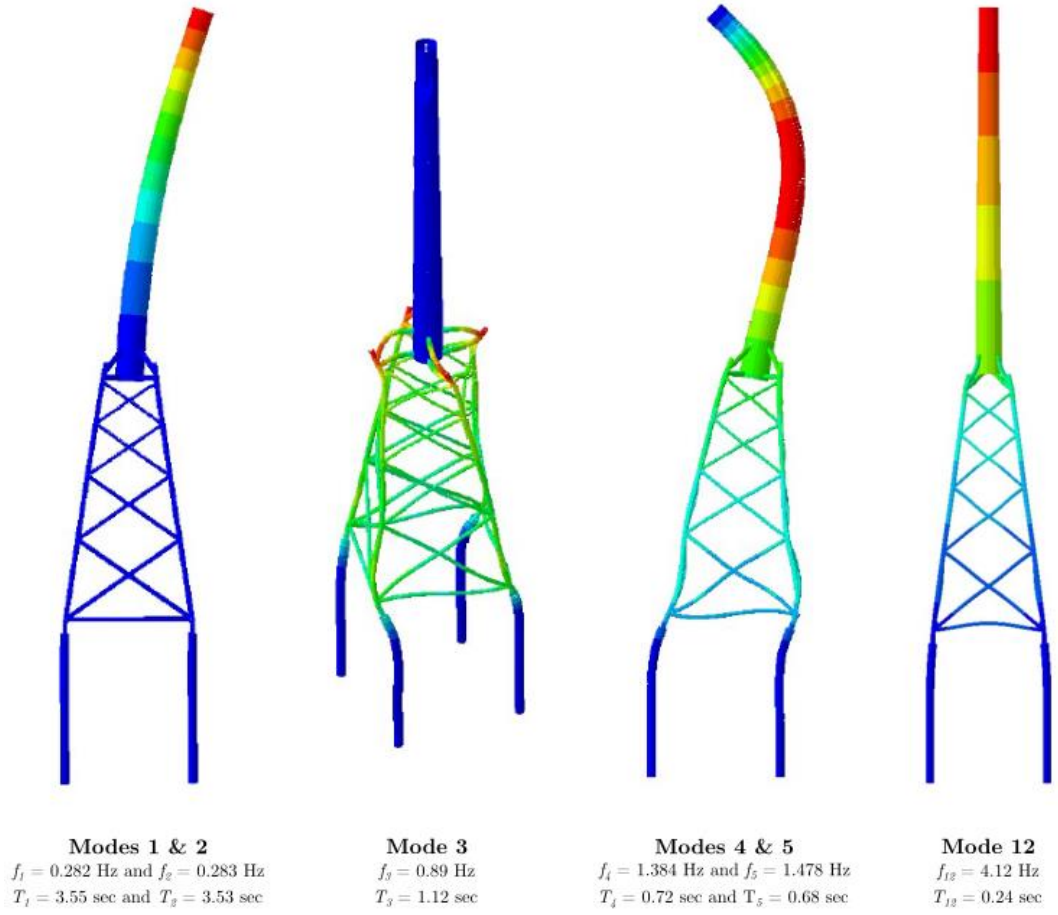

Figure 3: Mode shapes for: (a) first horizontal bending modes, (b) first torsional mode, (c) second horizontal bending modes, and (d) first vertical mode.

Generally, this step is of critical importance in the design phase where the natural frequencies of the turbine system should lie outside the range of applied mechanical and environmental loading during the operational state to avoid any undesirable resonance effects that can impose additional loading on the structure and significantly reduce its fatigue life. The vibration period of the first fore-aft and side-side modes is found to be around 3.5 sec corresponding to a modal mass participation ratio of around 30%. Additionally, it has been observed that it takes 7 modes to reach 85% of the total participation mass in the horizontal directions, while to reach 90%, 120 modes are required, which highlights the importance of considering higher modes for such structures. It can be also observed that generally the first bending modes in both directions are expected to be largely affected by the mass and stiffness distribution of the structure, while soil stiffness, both lateral and vertical, affects the higher bending, torsional and vertical modes. Also, due to the closely spaced periods of the first and second bending modes, mode coupling can be expected.

The effect of incorporating the aleatory variability in the structural steel Young's modulus and cross-section thickness deviation on the resulting vibration periods is then investigated. The steel Young's modulus is assumed to follow a lognormal distribution with a mean of 210 GPa and a

standard deviation of 6.3 GPa, while the thickness deviation is assumed to have a mean value of 1.2 mm and a standard deviation of 0.7 mm (JCSS, 2001; Thöns, Faber and Rücker, 2012), where thickness values for each segment of the tower and jacket were varied independently.

Mode no.	Description	Freq [Hz]	Period [sec]	Modal mass participation ratios [%]					
				x	y	z	Rx	Ry	Rz
1	1st Bending side-side (y-direction) mode	0.282	3.55	-	29.78	-	82.89	-	-
2	1st Bending fore-aft (x-direction) mode	0.283	3.53	30.21	-	-	-	83.11	-
3	1st Torsional mode	0.89	1.12	-	-	-	-	-	22.06
4	2nd Bending side-side (y-direction) mode	1.384	0.72	-	23.63	-	1.51	-	-
5	2nd Bending fore-aft (x-direction) mode	1.478	0.68	29.97	-	-	-	1.04	-
12	1st Vertical mode	4.12	0.24	-	-	59	-	-	-

Table 3: Mode frequencies, periods, and modal mass participation ratios for first and second horizontal bending modes, first torsional mode, and first vertical mode.

The variation of the resulting vibration periods for the modes of interest described above is evaluated via a simple Monte Carlo simulation, where the results showing the histograms and the fitted normal distributions are shown in Figure *4* and Table 4. It can be observed that the resulting coefficient of variation for the first five natural vibration periods is below 0.75% while it reaches around 1.1% for the first vertical mode vibration period indicating a minor influence that may be argued to be practically insignificant. However, care must be taken to include the variation in other parameters that could result in a high spread of the obtained values such as long-term degradation effects on the overall structural stiffness, long-term soil stiffness variation, numerical modelling assumptions especially the modelling of the soil domain, and others.

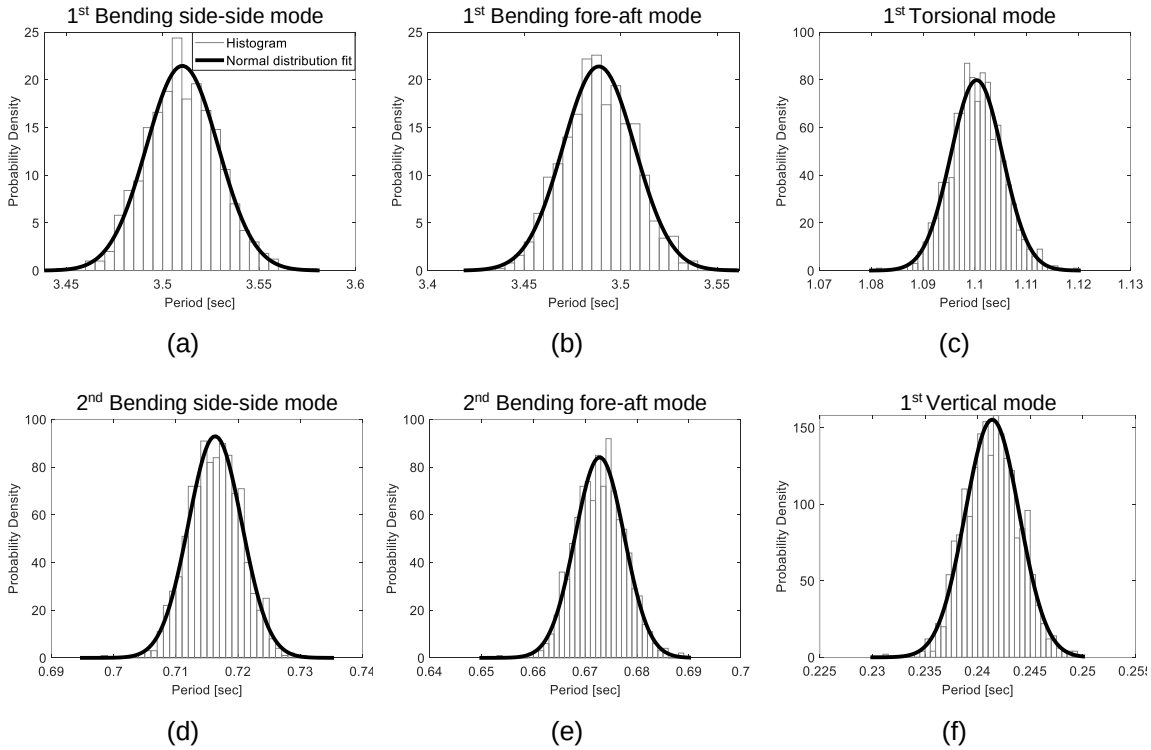

Figure 4: Normal distribution fit of the vibrational mode periods for: (a) 1st Bending side-side mode, (b) 1st Bending fore-aft mode (c) 1st torsional mode, (d) 2nd horizontal bending side-side mode, (e) 2nd horizontal bending fore-aft mode, and (f) 1st vertical mode.

Mode no.	Description	Mean [sec]	Standard Deviation [sec]	Coefficient of Variation [%]	5th Percentile	95th Percentile
1	1st Bending side-side (y-direction) mode	3.51	0.0186	0.53	3.48	3.54
2	1st Bending fore-aft (x-direction) mode	3.49	0.0186	0.53	3.46	3.52
3	1st Torsional mode	1.1	0.005	0.45	1.09	1.11
4	2nd Bending side-side (y-direction) mode	0.716	0.004	0.5	0.709	0.723
5	2nd Bending fore-aft (x-direction) mode	0.67	0.005	0.75	0.66	0.68
12	1st Vertical mode	0.24	0.0026	1.1	0.237	0.246

Table 4: INNWIND.EU 10 MW reference wind turbine statistical data for normal distribution fit of vibrational mode periods.

Seismic demand considerations

To obtain an insight into the expected level of seismic loading expected to act on such structures, the Eurocode 8 (CEN, 2004) Type 1 elastic horizontal response spectra for Site Classes A and D and damping ratios (ξ) of 2% and 5%, for a representative high seismicity site anchored for a PGA in rock of 0.4g are plotted as shown in Figure 5, in addition to the elastic vertical response spectrum for a damping ratio of 2%. The values of periods of interest for the first and second bending modes (Modes 1,2,4, and 5) and the first vertical mode (Mode 12) are also shown.

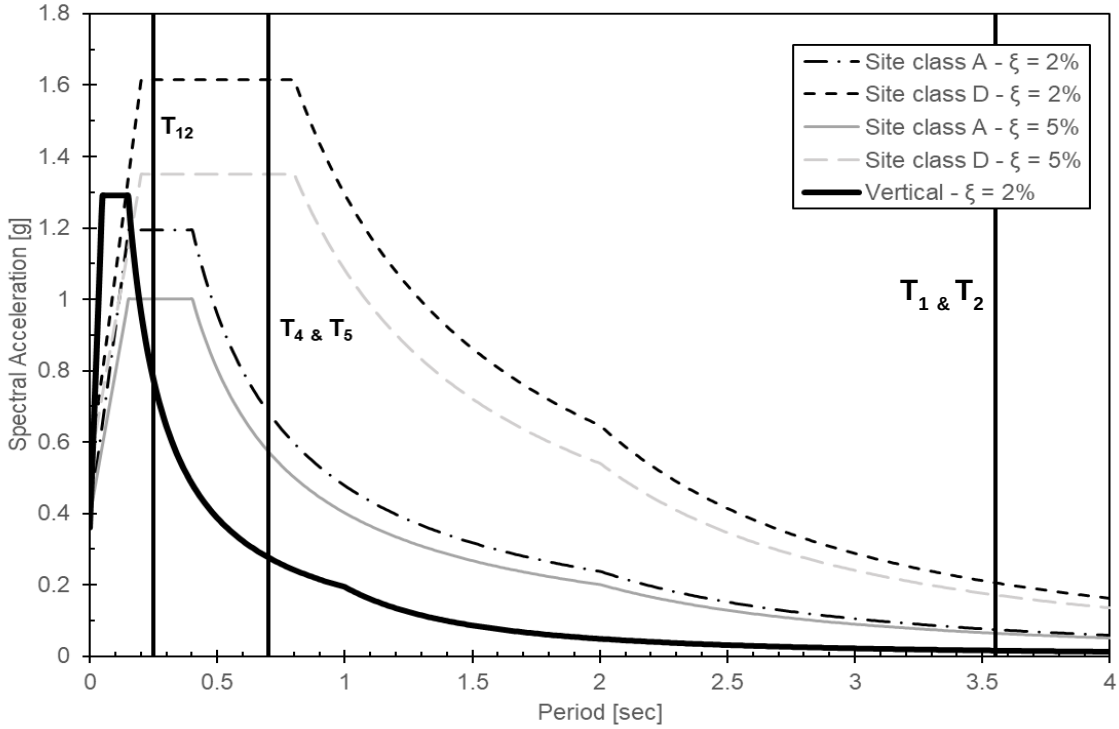

Figure 5: Eurocode 8 Type 1 spectra for different site classes and damping ratios, anchored for a PGA in rock of 0.4g, and values of periods of interest for first and second bending modes (Modes 1,2,4, and 5) and first vertical mode (Mode 12).

The choice of representative damping ratios to be used in the design and assessment of offshore wind turbines has been characterised by a varying range reflecting the uncertainties of estimating such values and their variation depending on the damping source for the various operational states and loading directions (Chen and Duffour, 2018). For example, structural damping can vary from 0.2% to 1.5%, and hydrodynamic damping can range from 0.11% to 0.39% and may reach

1% (Chen and Duffour, 2018; DNV, 2021). Soil damping has been reported in the range of 0.17% to 1.3% and can reach 4% (Chen and Duffour, 2018; DNV, 2021). Aerodynamic damping values depend on the operational state of the turbine, where for parked turbines, values in the range of 0.08% ‐ 0.24% are reported. On the other hand, for operating turbines, a large variation can be observed as it is a function of wind and rotor speed, in addition to vibration direction, whether in the side-side or fore-aft direction, which makes the damping value, in this case, dependent on the loading, and cannot just be regarded as a system property independent of the wind loading condition (Chen and Duffour, 2018). Additionally, in characterising the values of the damping ratios, it has been reported that the vibration response appears to be dominated by the first bending mode, which makes the above-mentioned values representative of first-mode damping ratios (Chen and Duffour, 2018). In addition, reliable values for damping ratios are still needed for the next generation of large-scale wind turbines for different substructure configurations. In this initial assessment, a damping ratio of 2% is chosen to be representative of the parked state of the turbine and operational state in the side-side direction, and the vertical mode, while a value of 5% is assumed for the operational state in the fore-aft direction. In addition, spectra for rock sites (Type A) and loose-to-medium cohesionless soil (Type D) are chosen as bounds for different representative site conditions.

It can be seen from Figure 5 that for the long-period first bending modes, spectral acceleration values are non-negligible especially for Site Class D due to unfavourable site amplification effects. In addition, the second bending modes vibration periods fall within the region of peak spectral acceleration for type D and relatively high values for type A. Moreover, the vertical mode vibration period falls in close vicinity of the peak vertical spectral acceleration values indicating the high vulnerability of such structures under vertical excitations.

Conclusions

Offshore wind energy farms are continuously growing to be a major source of clean renewable energy, where vital structures have been recently constructed in seismically active regions globally, along with ambitious future expansion plans in seismically active regions. There has been a relative lack of information on the long-term performance of large-scale offshore wind turbines under earthquake loading. This study focused on the assessment of the dynamic characteristics of relevance to the seismic performance of large-scale jacket-supported turbines of rated power of and exceeding 10 MW, which represents the future trend of offshore wind developments and have received little attention in the literature compared to monopile-supported offshore turbines. The performance of a four-legged, x-braced reference jacket structure supporting a 10 MW turbine constructed in a layered sand soil profile was investigated and initial insights into the seismic design and assessment that would enable the proper evaluation of the seismic response of such structural systems were presented.

References

API (2007), *API-RP-2A-WSD - Recommended Practice for Planning, Designing and Constructing Fixed Offshore Platforms—Working Stress Design*. American Petroleum Institute.

Bak, C. *et al.* (2013), 'Design and performance of a 10 MW wind turbine', *Wind Energy*, 124.

Bhattacharya, S. *et al.* (2021), 'Seismic Design of Offshore Wind Turbines: Good, Bad and Unknowns', *Energies*, 14(12), p. 3496. Available at: https://doi.org/10.3390/en14123496.

CEN (2004), *EN 1998-1 - Eurocode 8: Design of structures for earthquake resistance - Part 1: General Rules, seismic actions and rules for buildings*. Brussels: European Committee for Standardisation.

Chen, C. and Duffour, P. (2018), 'Modelling damping sources in monopile-supported offshore wind turbines', *Wind Energy*, 21(11), pp. 1121–1140. Available at: https://doi.org/10.1002/we.2218.

Dassault Systèmes (2022), ABAQUS FEA Analysis user's manual, Version 2022. Dassault Systèmes Simulia Corp.

DNV (2021), *DNV-RP-0585 - Seismic design of wind power plants*. Oslo, Norway: Det Norske Veritas Group.

GWEC (2022), *Global Wind Energy Report 2022*. Brussels, Belgium: Global Wind Energy Council.

JCSS (2001), *JCSS Model Code*. Brussels: European Committee for Standardisation.

Jensen, P.H. *et al.* (2017), *INNWIND.EU Final Report - LCOE reduction for the next generation offshore wind turbines*.

Thöns, S., Faber, M.H. and Rücker, W. (2012), 'Ultimate Limit State Model Basis for Assessment of Offshore Wind Energy Converters', *Journal of Offshore Mechanics and Arctic Engineering*, 134(3). Available at: https://doi.org/10.1115/1.4004513.

Von Borstel, T. (2013), *INNWIND.EU Design Report – Reference Jacket*. D4.3.1.

WFA (2022), *Global Offshore Wind Report*. Hamburg, Germany: World Forum Offshore Wind.